Bulletin of Electrical Engineering and Informatics
Vol. 12, No. 6, December 2023, pp. 3311~3324
ISSN: 2302-9285, DOI: 10.11591/eei.v12i6.6027

Anti-windup modified proportional integral derivative controller for a rotary switched reluctance actuator

Mariam Md Ghazaly[1], Siau Ping Tee[1], Nasharuddin Zainal[2]
[1]Center for Robotics and Industrial Automation (CeRIA), Fakulti Kejuruteraan Elektrik, Universiti Teknikal Malaysia Melaka, Melaka, Malaysia
[2]Department of Electrical, Electronic, and Systems Engineering, Faculty of Engineering and Built Environment, Universiti Kebangsaan Malaysia, Bangi, Malaysia

Article Info

Article history:

Received Feb 16, 2023
Revised Jun 4, 2023
Accepted Jul 13, 2023

Keywords:

Anti-windup
Fully aligned position
Intermediate alignmed position
Modified proportional integral derivative controller
Rotary switching reluctance actuator

ABSTRACT

Over the last decade, industrial applications and promising research domains including robotics and automotive engineering have adopted the rotary switched reluctance actuator (SRA). SRA's fault tolerance, simple, strong structure, and high-frequency operation make it popular. However, the SRA's nonlinear magnetic flux flow and saturation operation negate its benefits. Several control systems have been developed; however, they often need extensive mechanism models and advanced control theory, making them impracticable. This paper proposes a modified proportional integral derivative (PID) controller to evaluate the control performance, which comprises of PID controller with an anti-windup, a linearizer unit, and switching mechanism to activate the SRA phases. The linearizer unit aids to compensate for the non-linear current-displacement relationship. The anti-windup element helps to halt the integral action during the starting motion. At the fully aligned position, 60°, the modified PID reduced positioning steady-state error by 4.3 times at 76.9%, overshoot by 48.8%, and settling time by 25.3%. Both the modified PID and conventional PID showed zero steady-state error at intermediate position, 70°, however the modified PID controller depicted an improved percentage overshoot by 54.5% and settling time by 74.5%. The results show that the modified PID outperforms conventional PID in transient response, steady-state error, overshoot, and settling time.

Corresponding Author:

Mariam Md Ghazaly
Fakulti Kejuruteraan Elektrik, Universiti Teknikal Malaysia Melaka
Hang Tuah Jaya, 76100 Durian Tunggal, Melaka, Malaysia
Email: mariam@utem.edu.my

1. INTRODUCTION

Switched reluctance actuators (SRAs) are electromagnetic machines that convert electrical energy to magnetic field and generate electromagnetic force to drive a mechanical part (rotational or linear motion). Electromagnetic actuation in optical electromechanical systems (MOEMS) can provide large, long-range forces for industrial applications like magnetic matrix array of micro-switches for optical network and magnetostrictive scanner for automobile obstacle detection [1]–[4]. The permanent magnet (PM) in electromagnetic actuators makes bi-stability easy, and the pulse of excitation current maintains actuation positions through magnetic field interactions. Microelectromechanical systems (MEMS) use electromagnetic actuators for nanometer-precision positioning stages and medical laser scanners. However, electromagnetic actuators' complex design requires PMs, which is their biggest drawback. High-speed PM excitation dissipates power and reduces actuator efficiency [1], in which the SRA able to improve this shortcoming.

The rotary SRA is an electromagnetic actuator, but its simple, robust structure allows it to operate at higher temperatures without expensive PMs. The double stator SRA, multilayer SRA, and segmental rotor SRA are advanced rotary SRA design structures that increase torque and eliminate torque ripple. Reverting to the basic design of rotary SRA, the actuator has three main components: the rotor, stator, and coil windings, whereby a typical rotary SRA consist of 6/4 stator and rotor poles. These number of poles affects rotary SRA acoustics. More stator and rotor poles reduce noise, vibration, radial force and higher stator-rotor pole ratios improve actuation torque [5]. When a sequential excitation scheme is initiated, the rotor rotates to align with the excited stator poles to form the magnetic flux path with the least reluctance. Because air resists magnetic flux in the rotary SRA, lowering output torque, the air gap should be as small as possible. The air gap must be large enough to allow smooth rotation without rotor-stator contact. Because the SRA lacks rotor winding, the windings are formed externally and inserted into the stator, simplifying construction. The SRA has high power factor and efficiency in high-speed modes. This makes SRA suitable for hybrid electrical vehicle (HEV) applications [6], which could revolutionise the industry. HEVs are greener and cheaper to maintain than gas-powered cars. Rotary SRA is also suitable for wind power systems due to its simple, robust, low-cost structure, and lack of speed multiplication system. The rotary SRA can also be used to replace PM stepper motors in robotic joints and manipulators [7].

Despite its benefits, the rotary SRA has some drawbacks in its application. Due to magnetic flux linkage and magnetic saturation, rotary SRA is intricately non-linear [8]–[13]. The non-linear rotary SRA makes analytical modelling difficult. Control schemes require magnetization curve measurements or finite element predictions, complicating the controller design. These factors make real-time rotary SRA motion control difficult and inaccurate. At present, there are numerous control methods proposed and established for motion control of linear SRA. However, for rotary SRA it is limited. Most of these early works used model-based control, which improves performance but depends on system modelling accuracy and quality [14]–[18]. Classical control uses the proportional integral derivative (PID) because of its simple design and high applicability for industrial operations. Due to the linear controllers, unfortunately the PID control method performs poorly with non-linear type mechanisms. Model-free controllers such as intelligent and hybrid [19]–[23] were also used in past researches, whereby the control architecture is simpler than with model-based controllers because the controller decision making can accommodate system uncertainties and variations. Nevertheless, knowledge of control theory and a time-consuming design process are both prerequisites for working with these controllers. As a result, the methodology of a simple and practical control strategy [24], [25] for a rotary SRA will be discussed in this paper. By including a linearize unit and anti-windup, this control strategy modifies the structure of a PID as the fundamental controller.

2. METHOD

This section discusses the dimensions and construction parameters of the rotary SRA, followed by a detailed SRA experimental setup. The experimental excitation sequence which consists of three (3) phases are discussed in detail with the SRA's working range between 0° to 75°. To evaluate the control performance of the SRA, the procedure to design the modified PID control scheme is elaborated. The modified PID control scheme comprises of a PID controller with an anti-windup, a linearizer unit, and switching mechanism to activate the SRA phases.

2.1. Switched reluctance actuator prototype and experimental setup

In this paper, the SRA prototype uses a modified PID control to validate its practical control scheme. The SRA continuous motion ranges from 0° to 360°. The rotary SRA design uses Malaysian-available materials and no rare PMs. The material used for the stator and rotor are S45C medium-carbon steel. Figure 1 shows the SRA rotor and stator dimensions. Figure 2 and Table 1 show the optimised design parameters using finite element method (FEM) analysis. The initial stator-rotor air gap is 0.2 mm, however the SRA prototype air gaps vary from 0.22 to 0.23 mm due to fabrication tolerances. To prevent electricity from reaching the stator, each stator tooth is insulated with 0.1 mm DuPont NOMEX paper type 410 as shown in Figure 3. The stator tooth is wrapped 60 times with 0.1 mm copper wire. The coil windings are insulated to prevent electricity flow between phases and pack tightly into the stator teeth.

The fully assembled SRA setup consists of several components other than the stator, rotor, and coil windings. Figure 4 depicts the aluminum-base SRA experimental setup. The experimental setup includes a host PC, micro-box DSP unit, 3 high current amplifiers (Kikusui PBZ60-6.7 and Accel TS250), and the fully assembled SRA setup. The SRA stator is mounted on an acrylic-aluminum holder to prevent electrical conductivity. High-precision ball bearings with housing keep the stator and rotor in line. A scancon rotary incremental encoder with 0.1° resolution is located on one end of the shaft, and a protractor and pointer are located on the other. To precisely measure rotor displacement, a duratool USB microscope is placed in front

of the protractor. Bolts, nuts, and screws made of plastic or steel coated with black oxide reduce electrical conductivity and secure all components.

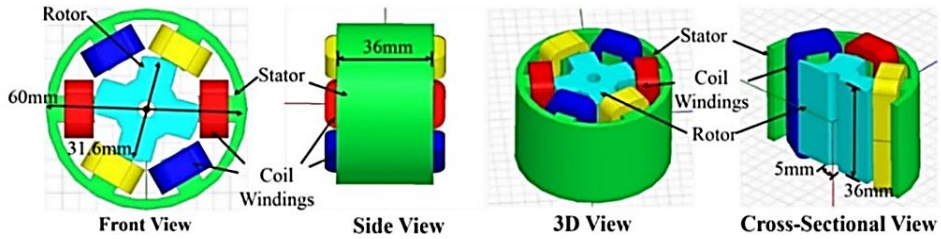

Figure 1. Dimensions of SRA in different views

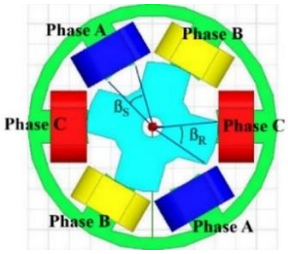

Figure 2. SRA design parameters

Table 1. SRA design parameters

Parameters	Value
Stator-to-rotor poles ratio, S:R	6:4
Air gap	0.23 mm
Winding turns	60
Arc angle, $ß_S$ / $ß_R$	29°/40°

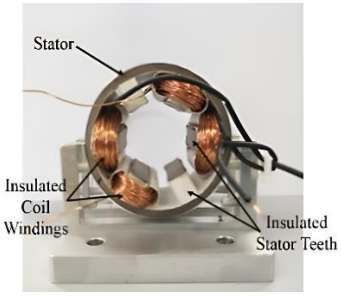

Figure 3. Insulated SRA stator teeth and coil windings

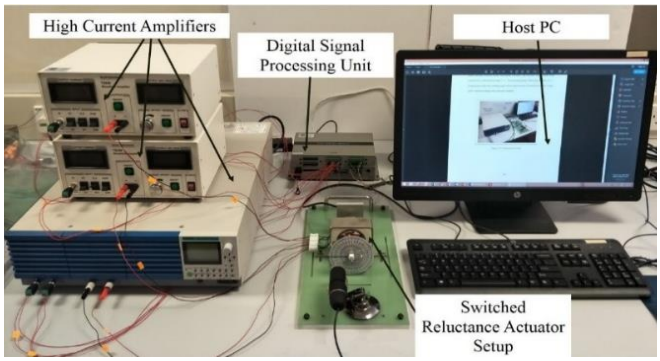

Figure 4. SRA experimental setup

2.2. Rotary switched reluctance actuator excitation phase

All experiments will be carried out in the SRA's working range of 0° to 75° and will employ one of the three phases. Due to air gap non-uniformity and fabrication constraints, phase ABC excitation can only rotate the rotor from 0° to 75°, rather than 0° to 90°, as shown in Figure 5(a) for the counter-clockwise (counter-CW) rotation and Figure 5(b) for the clockwise (CW) rotation. When no current is applied and the SRA is demagnetized, the rotor can only achieve a fixed position manually due to gravity's pull. Furthermore, 0° is the position at which the rotor is fully aligned with the previous phase (phase C) before activating the first phase (phase A). Manual positioning of the rotor to starting position 0° is accomplished in the SRA setup using a digital microscope, protractor, and pointer, as shown in Figure 6. After each experiment, a customised waveform of positive and negative step signals is applied to each phase of the SRA system to discharging the accumulated magnetic flux within the core as shown in Figure 7. The discharging process is carried out primarily to ensure that the rotor can be manually repositioned to 0°. This procedure also serves as an extra precautionary measure to ensure that the SRA is not saturated.

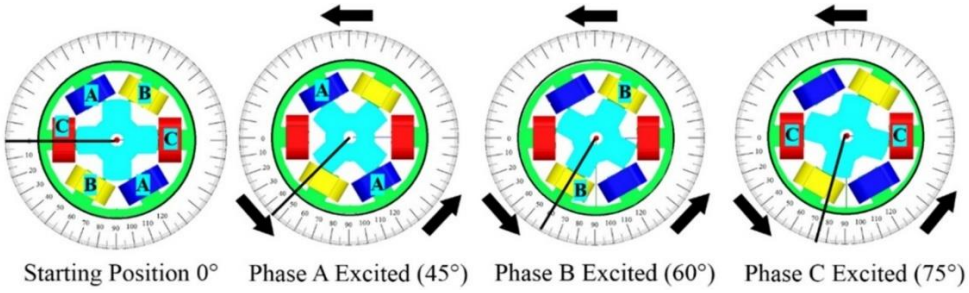

(a)

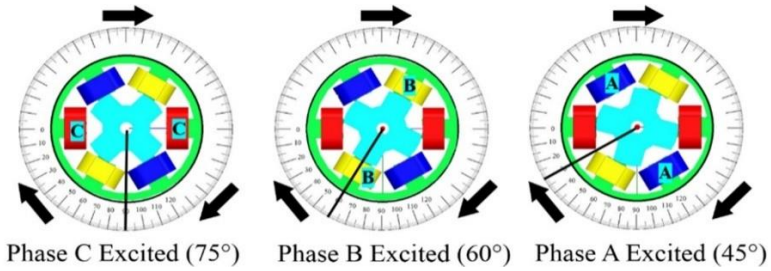

(b)

Figure 5. SRA actual positions through sequential phase excitation: (a) counter-CW rotation and (b) CW rotation

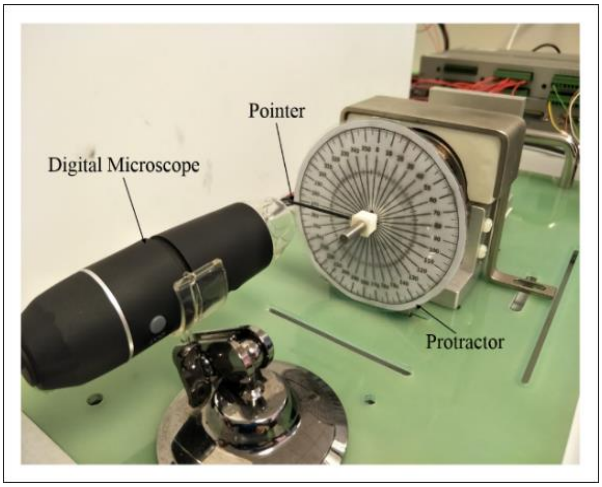

Figure 6. Setup to position the rotor at 0°

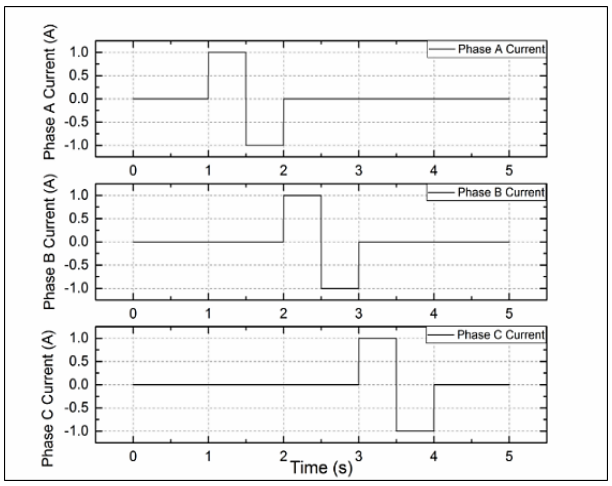

Figure 7. Customized waveforms for discharge of magnetic flux in SRA

2.3. Design procedure of modified proportional integral derivative control scheme

Figure 8 shows the proposed modified PID controller, which comprises of PID controller with an anti-windup, a linearizer unit, and simple switching mechanism to activate the SRA phases shown in Table 2. This control scheme activates phases based on the rotary displacement, error, and reference values. Table 2 shows the CW and anticlockwise (ACW) rotary displacement, and excitation phases. In an uncompensated system, the SRA oscillates and loses accuracy during point-to-point motion. The uncompensated system cannot consistently maintain and achieve a settling displacement because the SRA constantly excites two phases sequentially to reach the reference position. Hence to solve this, the PID controller is implemented as the fundamental controller. The PID controller was design using Ziegler-Nichols tuning method at a sampling rate of 1 kHz. Ziegler-Nichols tuning method heuristically determines K_P, K_I, and K_D values. By setting K_I and K_D values to 0, the K_P value is increased from 0 until the SRA displayed sustained oscillations as shown in Figure 9. This K_P value is known as the ultimate gain, K_U, which is 2.7. The K_U value must be the smallest value of K_P for the control loop to achieve sustained oscillation. The oscillation period or ultimate period, P_U is also obtained which is 0.184 s. The calculations as shown in Table 3 is completed using the acquired K_U and P_U values. The final calculations for K_P, K_I, and K_D values are completed and the initial PID gain values using Ziegler-Nichols method are shown in Table 4.

However, because the SRA is a highly nonlinear system, the structure of the modified PID controller must include a linearizer unit. The linearizer unit compensates for the SRA system's non-linear current-displacement relationship. To achieve better positioning results, this component acts as a lookup table for the current value for each phase. The construction of the linearizer unit begins with determining the rotary displacement of the SRA using open-loop responses. Current values ranging from 0.5 to 2 A, with intervals of 0.1 A, are sequentially applied to SRA phases to generate reciprocating motion between 45° and 75°. This method makes it simple to obtain the displacement characteristics of all three phases. Because lower current values do not provide enough energy for the SRA to achieve a stable response, the excitation current begins at 0.5 A. The current is limited to 2 A because higher values may cause the winding coils to overheat and burn. Each current value will correspond to their respective steady-state displacement using the displacement responses in the reciprocating motion. In this manner, a collection of current values ranging from 0.5 to 2 A against their respective displacement is obtained in a graph for each phase. For each graph, an equation defining the relationship is obtained. Each equation will serve as the linearizer unit, compensating for the non-linear characteristics of SRA for each individual phase.

Using a conventional PID controller, there is the issue where the control signal becomes saturated due to error accumulation of the integral term. This is problematic as such situation forces the linearizer to lose its function because the maximum output current will always be selected and supplied to the SRA regardless of the actual error of the system. Considering the ease of implementation, a conditionally freeze integrator is added to the compensated closed-loop system in order to avoid the saturation of PID signal due to the integral term. In (1) governs the anti-windup element's integral input. The value of u_{PID} is the maximum PID signal value at 2 A current which is 20.225°. The linearizer look-up table easily determines the highest value of the three linearizer units at 2 A since the SRA is a single-feedback closed-loop system. When two conditions are met, the anti-windup element freezes the integral value: i) the modulus sum of proportional, integral, and derivative control signals exceeds the maximum value and ii) the product of error and integral control signal

exceeds or equals zero; otherwise, the integral term functions normally. The conditional integrator is chosen because the rule can be modified to fit the SRA system. The integral term is halted when the rotary response starts because the PID signal is saturated by the proportional term and only acts when approaching the steady-state phase. This effectively reduces overshoot while also significantly reducing error and settling time as the steady-state phase approaches. The modified PID controller in Table 4 is fine-tuned to achieve the best possible performance for the SRA system. The K_P, K_I, and K_D values are optimised through experimental work using the initial PID gain values from the Ziegler-Nichols method. Table 5 shows final PID gain values.

$$\Delta u_i = \begin{cases} 0, & |u_P + u_i + u_D| > u_S \ \ and \ \ e \cdot u_i \geq 0 \\ e, & otherwise \end{cases} \quad (1)$$

Where u_P is proportional control signal; u_i is integral control signal; Δu_i is change rate of u_i; u_D is derivative control signal; u_{PID} is maximum value of PID signal at 2 A; and e is error

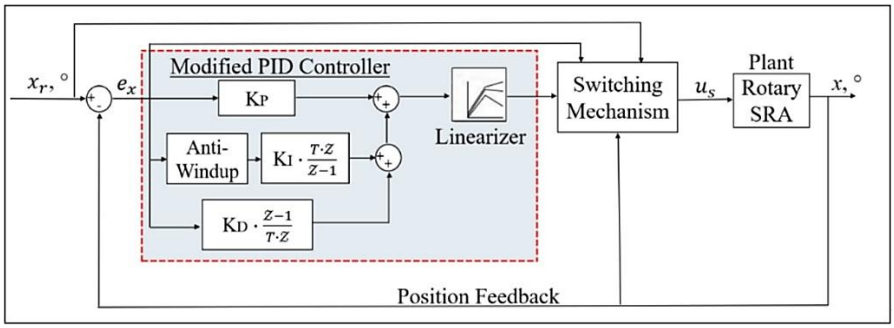

Figure 8. Block diagram of modified PID controller

Table 2. Excitation phases for CW and ACW rotation

Rotary displacement	CW phase	ACW phase
0°-30°	A	C
30°-60°	B	A
60°-90°	C	B
90°-120°	A	C
120°-150°	B	A
150°-180°	C	B
180°-210°	A	C
210°-240°	B	A
240°-270°	C	B
270°-300°	A	C
300°-330°	B	A
330°-360°	C	B

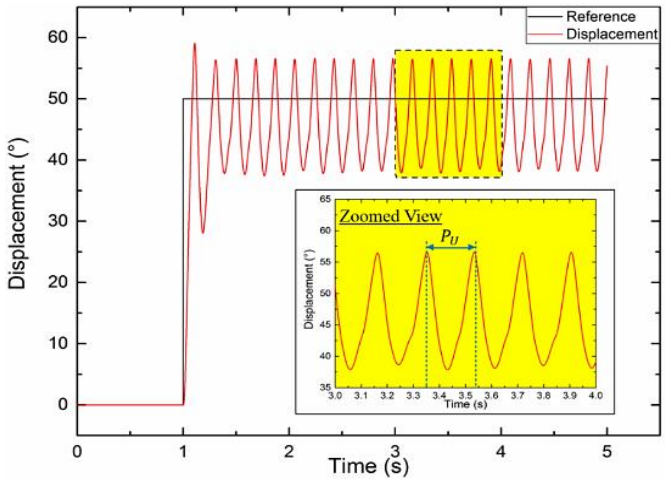

Figure 9. Step response at ultimate gain, K_U=2.7

Table 3. Controller parameters using Ziegler-Nichols method

	K_P	T_I	T_D
P controller	$0.5\times K_U=1.35$	∞	0
PI controller	$0.45\times K_U=1.22$	$\frac{P_U}{1.2}=0.15$	0
PID controller	$0.6\times K_U=1.62$	$0.5\times P_U=0.092$	$0.125\times P_U=0.02$

Table 4. Initial PID gain values

PID gain	Value
K_P (°)	0.6 Ku=1.62
K_I (°s^{-1})	$\frac{K_P}{T_I}=17.6$
K_D (°s)	$K_P\times T_D=0.03$

Table 5. Final PID gain values for the modified PID controller

PID gain	Value
K_P (°)	2.02
K_I (°s^{-1})	22
K_D (°s)	0.07

3. RESULTS AND DISCUSSION

In this section, the construction of the linearizer unit for each phase is discussed, including the curve-fitting the current-displacement relationship to obtain the linearizer equation for phase A, B, and C. The modified PID controller performance will be discussed and evaluated using two references, i.e. i) fully aligned and ii) intermediate reference positions. The results will be compared using the conventional PID controller to verify the benefits of the modified PID controller for the SRA application. For the fully aligned reference position, the SRA is evaluated at references positions 60° and 75°. While for the intermediate reference position, the control performances were evaluated at 55° and 70°.

3.1. Linerizer unit construction

The linearize unit provides a non-linear current-displacement relationship for the SRA system and serves as a lookup table to provide the suitable current excitation for accurate positioning in a closed-loop system. Sequential excitation of phase A-B-C and vice versa initiates a reciprocating motion in the range of 45° to 75°. Each phase is excited with the same current values, ranging from 0.5 to 2 A for activation period of 1.5 s, starting at time, T=1 s. Figure 10 shows the example of the reciprocating motion for current values 2 A. The reciprocating motion not only provided a displacement value for each current value, but it also demonstrated that phase A and C excitation are unable to achieve the expected displacement of 30° and 90°, respectively. When phase A is excited, the rotor only moves about 45°, whereas phase C produces a 75° displacement. This problem is caused by hardware fabrication tolerance and air gap non-uniformity. However, phase B did not exhibit this problem because its rotary response is very close to the expected displacement of 60°. As a result, the stator and rotor fully aligned positions for phases A and C are 45° and 75°, respectively.

The relationship between varying current values and displacement is obtained in graphs according to each phase using the displacement responses in the reciprocating motion shown in Figure 11. The displacement for each current value is determined by selecting the reciprocating response that is closest to the average value among the five repetitions. Because phase A and C are only involved in either CW or counter-CW rotation, they each have one graph shown in Figures 11(a) and (d), respectively. Phase B, on the other hand, has two displacement-current graphs that rotate CW and ACW, as shown in Figures 11(b) and (c). The graphs show that the displacement versus current revealed a nearly identical relationship between them. In general, every 0.1 A increase in current from 0 to 1 A results in a significant increase in displacement. However, from 1 to 2 A, the same 0.1 A increase in current results in a smaller increase in displacement. Except for CW phase B, which showed slight displacement spikes at 0.6 and 1.1 A, all three phases exhibited a relationship similar to that of an exponential graph. A notable feature is that as the current values near the maximum at 2 A, the displacement decreases slightly and remains constant across all phases.

Figure 11 shows that curve fitting analysis is required to obtain an equation defining the displacement-current relationship for each phase. The Boltzmann model function is used to fit the displacement-current graph. Because the displacement changes little when the current approaches 2 A, the Boltzmann function is appropriate for expressing the displacement-current relationship. Furthermore, when the current approached 2 A, the displacement showed a minor decrement. However, U-shaped curves cannot be used

in the curve fitting equation because they would produce two different current values with the same displacement. If such equations are used in the linearizer unit, this will result in conflicting values in the lookup table.

The equation representing the graphs in Figure 11 are shown in (2)–(5), will be used in the linearizer unit in designing the modified PID. However, (2)-(5) express the displacement value in terms of the current value, whereas the compensated closed-loop system requires the current value to be expressed in terms of the displacement value. As a result, the equations for the corresponding phases are inversed, as illustrated in (6)-(9). Using (6), the linearizer for phase A is constructed as shown in Figure 12(a). In the case of phase B, the linearizer graph shown in Figure 12(b) is constructed by combining (7) for positive displacement and (8) for negative displacement. This is because phase B is involved in both CW and ACW rotation. The linerizer for phase C is the mirrored version of phase A shown in Figures 12(c) with respect to the y-axis to reflect the negative displacement side. In Figure 12, the linearizers express current values in terms of displacement; for example, a current value of 0.26 A must be excited in order for phase A of the SRA system to achieve 5°.

$$Y_A=16.964-\left(\frac{23.472}{1+\exp\left(\frac{x-0.299}{0.312}\right)}\right) \quad (2)$$

$$Y_{B\,(cw)}=15.081-\left(\frac{27.822}{1+\exp\left(\frac{x-0.071}{0.414}\right)}\right) \quad (3)$$

$$Y_{B\,(ccw)}=-22.828\times\left(\exp\left(\frac{-x}{0.894}\right)\right)+22.662 \quad (4)$$

$$Y_C=14.781-\left(\frac{20.674}{1+\exp\left(\frac{x-0.264}{0.287}\right)}\right) \quad (5)$$

$$Linearizer_A=0.299+0.312\times\ln\left(\frac{23.472}{16.964-x}-1\right) \quad (6)$$

$$Linearizer_{B\,(cw)}=-0.894\times\ln\left(\frac{22.662-x}{22.828}\right) \quad (7)$$

$$Linearizer_{B\,(ccw)}=0.299+0.312\times\ln\left(\frac{23.472}{16.964-x}-1\right) \quad (8)$$

$$Linearizer_C=0.264+0.287\times\ln\left(\frac{20.674}{14.781-x}-1\right) \quad (9)$$

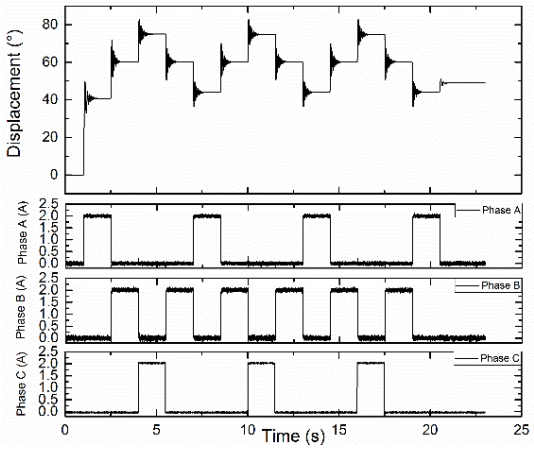

Figure 10. Reciprocating motion using 2 A current

3.2. Performance evaluation: fully aligned vs intermediate positions

The modified PID controller was evaluated at two reference positions: fully aligned and intermediate positions. Both were compared to the conventional PID controller to demonstrate its efficacy. Table 6 lists the conventional and modified PID controller parameters that was tuned. The SRA fully aligned positions involved in experimental references are 60° and 75°, respectively. At 60° and 75°, the rotor is fully aligned with phase C and phase A stators. Because torque is at its lowest when the rotor reaches the fully aligned position, these positions pose the greatest challenge in rotary SRA position control. Positioning errors are common because increasing the current using the corresponding phases produces no motion. Figure 13 shows the performances for

reference 60° and 75° positioning. Figure 13(a) shows that modified PID had less displacement response overshoot and oscillations than the PID. Modified PID reached a steady-state position of 59.9° with a 0.1° average error for a reference position of 60°. PID controller errors were 0.5°. The PID controller displacement exceeded 80.5° by 34.3%. The modified PID had 17.6% overshoot and 0.460 s settling time, better than the PID controller. Modified PID had an improved steady-state error by 4.3 times at reference 60°, 76.9%. The modified PID controller reduced overshoot and settling time by 2 and 1.3 times, improving 48.8% and 25.3%. For the reference position 75°, the modified PID controller eliminates oscillations shown in Figure 13(b). Additionally, modified PID had zero steady-state error, while PID had 0.5°. The PID controller displacement overshoot by 18% to 88.5°. However, modified PID reached 80.2° with a 6.9% overshoot. In contrast, the modified PID improved steady-state error and overshoot by 100% and 61.9%. The modified PID settled in 0.207 s versus the PID controller's 0.574 s. 2.8 times faster settling and 63.9% better with the modified PID controller. Tables 7 and 8 shows the transient parameters for reference 60° and 75°.

In compared to the fully aligned positon, the intermediate alignment at 55° and 70° is the position where rotor and stator is not aligned, whereby 55° is in between phases A and B, while 70° is in between B and C. From Figure 14, the intermediate positions depict a zero steady-state error. The linearizer unit significantly helps to improved displacement curve, overshoot, and settling time. Figure 14(a) shows that the modified PID controller outperformed the PID controller at 55° reference position. The PID controller had 38.6% overshoot, while modified PID achieve a 16.1% overshoot. The overshoot decreased by 2.4-fold and improved by 58.4%. The modified PID settled in 0.402 s, while the PID took 0.605 s to reach the setpoint, which shows that the modified PID improves by 33.5%. Figure 14(b) shows that the PID controller overshoot and oscillated at reference 75° before correcting to 70°. The modified PID responded smoothly to the reference input. It can be depicted that the modified PID outperformed PID with a 12% overshoot versus 26.3%. The overshoot decreased by 2.2-fold. The modified PID reduced settling time by 3.9 times, from 0.889 s to 0.227 s, in which 74.5% improvement. Tables 9 and 10 shows the transient parameters for reference 55° and 70°.

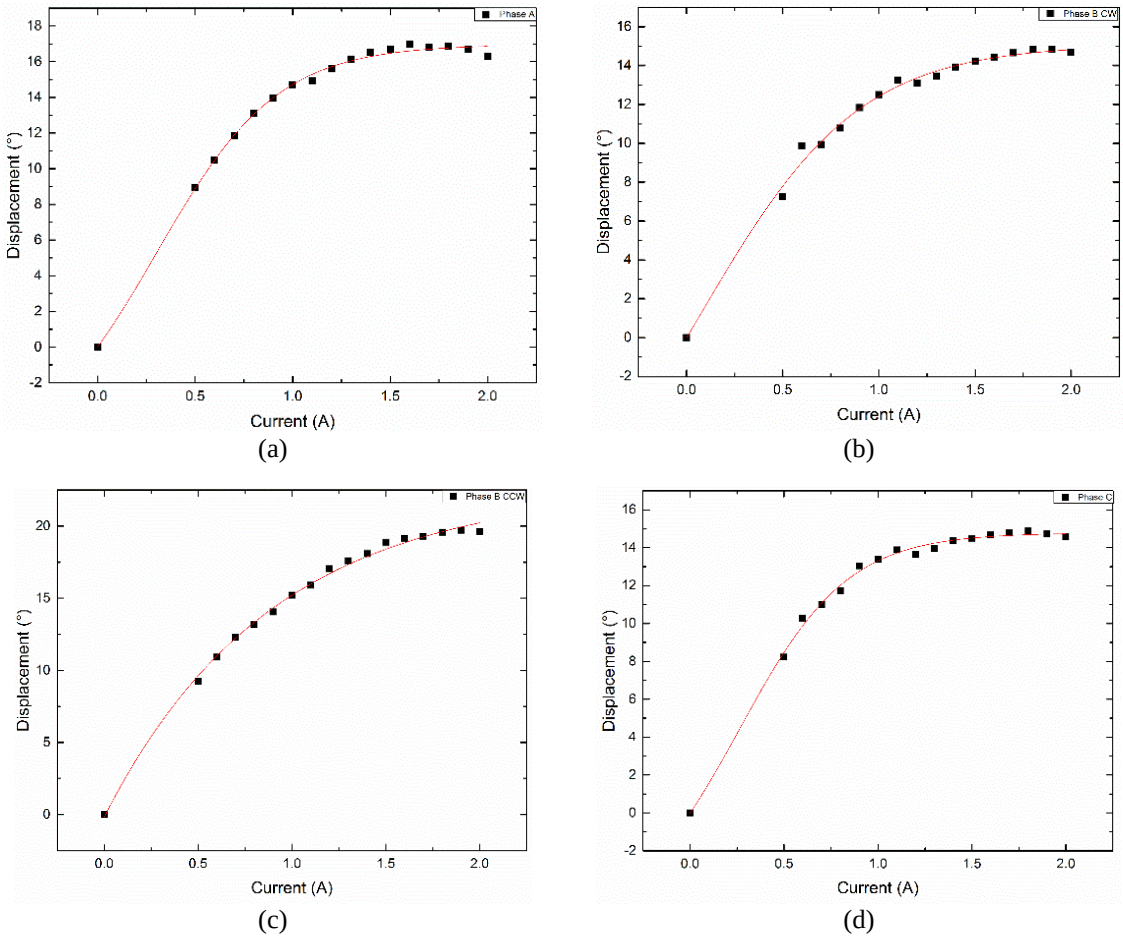

Figure 11. Relationship of displacement against current for (a) phase A, (b) phase B (CW), (c) phase B (counter-CW), and (d) phase C

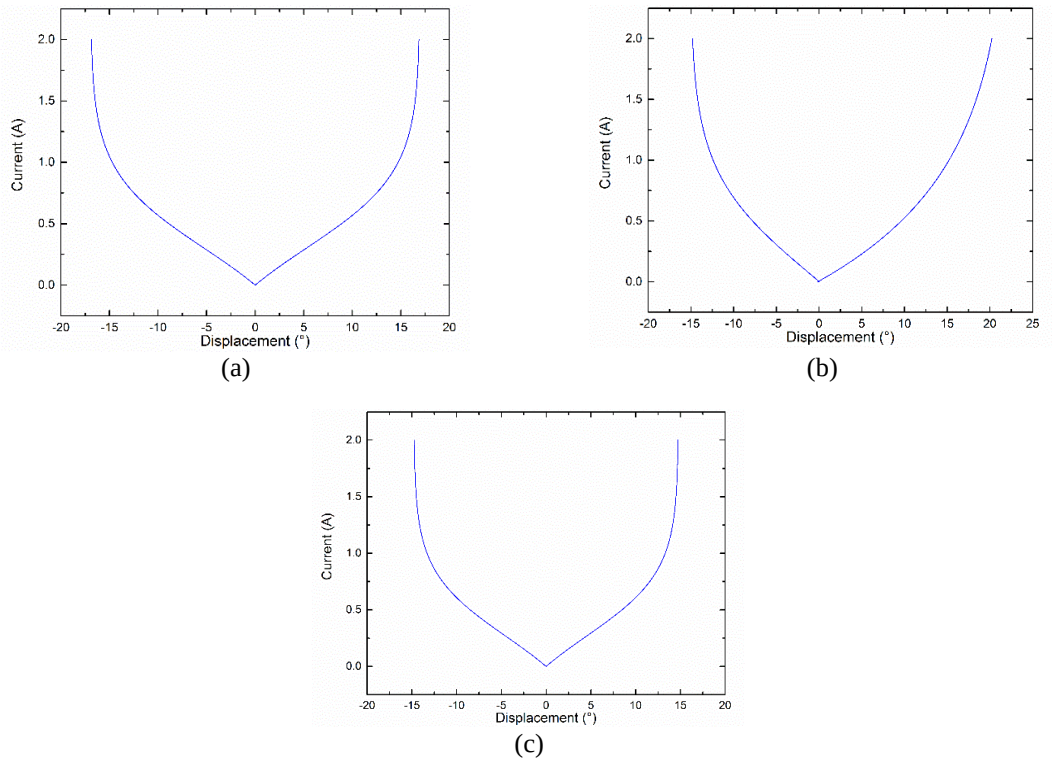

Figure 12. Linearizer for current-displacement relationship for (a) phase A, (b) phase B, and (c) phase C

Table 6. Controller parameters for conventional PID and modified PID controllers

PID gain	Modified PID	Conventional PID
K_P (°)	2.02	0.3
K_I (°s^{-1})	22	3.28
K_D (°s)	0.07	0.01

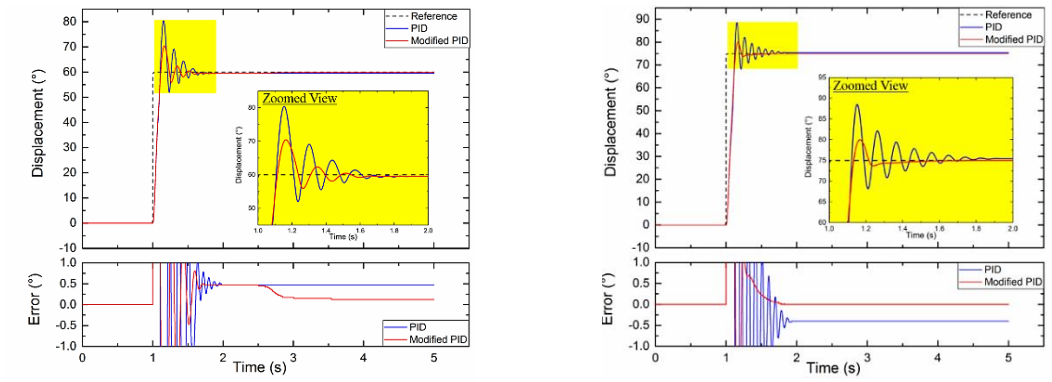

Figure 13. Comparative positioning result for modified PID and PID at fully align positions at (a) reference 60° and (b) reference 75°

Table 7. Transient parameters for modified PID and PID controller for 10 repeatability at reference 60°

Parameters		Reference 60° Modified PID	PID	Improvement (times/%)
Steady-state error (°)	Average	1.20×10^{-1}	5.20×10^{-1}	4.3/76.9
	Standard deviation	4.22×10^{-2}	4.22×10^{-2}	
Overshoot (%)	Average	1.76×10^{1}	3.43×10^{1}	2.0/48.8
	Standard deviation	2.18×10^{-1}	3.95×10^{-1}	
Settling time (s)	Average	4.60×10^{-1}	6.16×10^{-1}	1.3/25.3
	Standard deviation	3.41×10-^{3}	2.97×10^{-2}	

Table 8. Transient parameters for modified PID and PID controller for 10 repeatability at reference 75°

Parameters		Reference 75° Modified PID	PID	Improvement (times/%)
Steady-state error (°)	Average	0.00	4.50×10-1	-/100
	Standard deviation	0.00	5.27×10-1	
Overshoot (%)	Average	6.87×100	1.80×101	2.6/61.9
	Standard deviation	3.09×10-1	1.99×10-1	
Settling time (s)	Average	2.07×10-1	5.74×10-1	2.8/63.9
	Standard deviation	1.58×10-3	4.78×10-3	

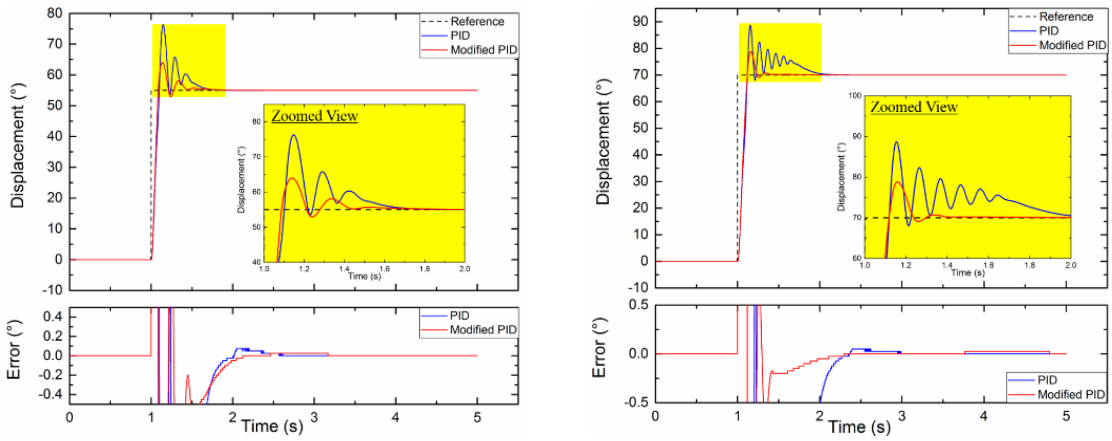

Figure 14. Comparative positioning result for modified PID and PID at intermediate positions at (a) reference 55° and (b) reference 70°

Table 9. Transient parameters for modified PID and PID controller for 10 repeatability at reference 55°

Parameters		Reference 55° Modified PID	PID	Improvement (times/%)
Steady-state error (°)	Average	0.00	0.00	0.0/0.0
	Standard deviation	0.00	0.00	
Overshoot (%)	Average	1.61×10^{1}	3.86×10^{1}	2.4/58.4
	Standard deviation	3.57×10^{-1}	6.62×10^{-1}	
Settling time (s)	Average	4.02×10^{-1}	6.05×10^{-1}	1.5/33.5
	Standard deviation	8.09×10^{-3}	9.70×10^{-3}	

Table 10. Transient parameters for modified PID and PID controller for 10 repeatability at reference 70°

Parameters		Reference 70° Modified PID	PID	Improvement (times/%)
Steady-state error (°)	Average	0.00	0.00	0.0/0.0
	Standard deviation	0.00	0.00	
Overshoot (%)	Average	1.20×10^{1}	2.63×10^{1}	2.2/54.5
	Standard deviation	8.74×10^{-1}	4.49×10^{-1}	
Settling time (s)	Average	2.27×10^{-1}	8.89×10^{-1}	3.9/74.5
	Standard deviation	4.70×10^{-3}	1.05×10^{-2}	

Based on the analysis, the modified PID controller performs better compared to the PID controller with the aid of a linearizer unit. Figure 15 shows both controllers' phase excitation at fully aligned position, 60° and intermediate position, 70°. When fully aligned positions were achieved, the PID controller demonstrated a significant reduction in steady-state error. This is because the torque decreases when approaching these positions, also known as dead zones, because the minimal torque refuses any further movement even when the corresponding aligned phase is excited. Figure 15(a) demonstrated that the excitation current of phase B by the PID controller easily reached saturation at 2 A, resulting in more overshoot and oscillations. The linearizer unit solves this problem by defining the current-displacement relationship to ensure appropriate excitation current based on the system's open-loop characteristics, which (modified PID's phase B current) is significantly lower than that of the PID controller, as shown in Figure 15(b). As a result, as the rotor approaches its fully aligned position, the positioning error can be reduced by applying more current. As shown in Figure 15(b), the modified PID registered lower current values for phases B and C, indicating a response closely tracing the reference input with less overshoot and settling time.

Aside from the linearizer unit, the anti-windup element had a significant impact on the displacement response. Although the conventional PID controller has anti-windup, its performance is inferior to that of the modified PID. When combined with the linearizer unit in the modified PID controller, the anti-windup element performs admirably. Figure 16 depicts the PID signal before entering the linearizer unit for two controllers, a modified PID controller with and without an anti-windup element for reference positions 60° and 70°, respectively. The absence of a linearizer unit in the conventional PID scheme is a significant disadvantage because there are no elements to define the non-linear SRA current-displacement relationship. Even if an anti-windup element were included, it would serve little to no purpose, as demonstrated by all previous positioning results. However, the role of anti-windup in the modified PID controller is notable, as shown in Figure 16(a) at fully aligned position, 60°, where the PID signal without anti-windup showed saturation beyond the limit until the experiment was terminated. The proportional and derivative terms in the PID signal with anti-windup, on the other hand, caused saturation at the start of motion. The integral action is currently frozen. Once the PID signal has reached its saturation point, the integral term only acts to reduce the steady-state error. Similarly, in Figure 16(b) at the intermediate position of 70°, the anti-windup element effectively reduces overshoot and improves settling time by freezing the integral action during the starting motion. In order to deliver optimal performance, the modified PID scheme requires both the linearizer unit and the anti-windup element.

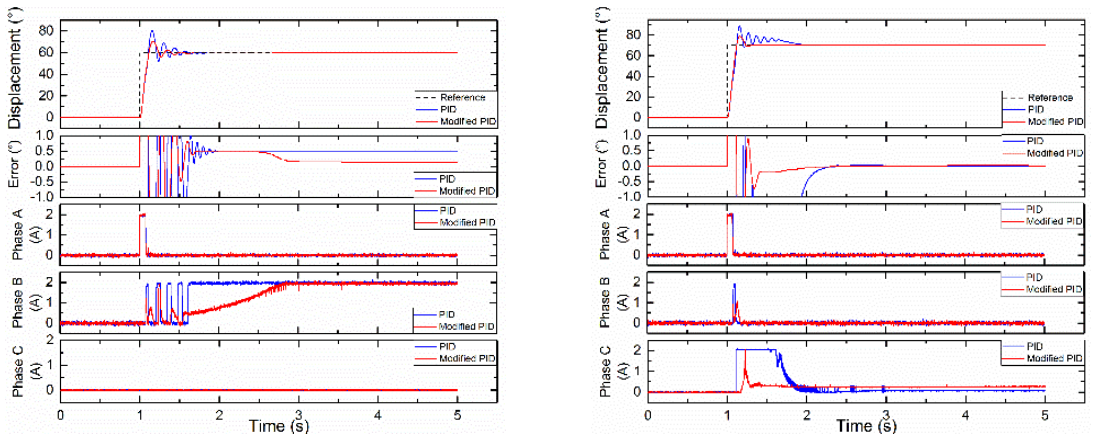

Figure 15. Effect of linearizer: comparative excitation current for different phases at (a) reference 60° (fully aligned position) and (b) reference 70° (intermediate position)

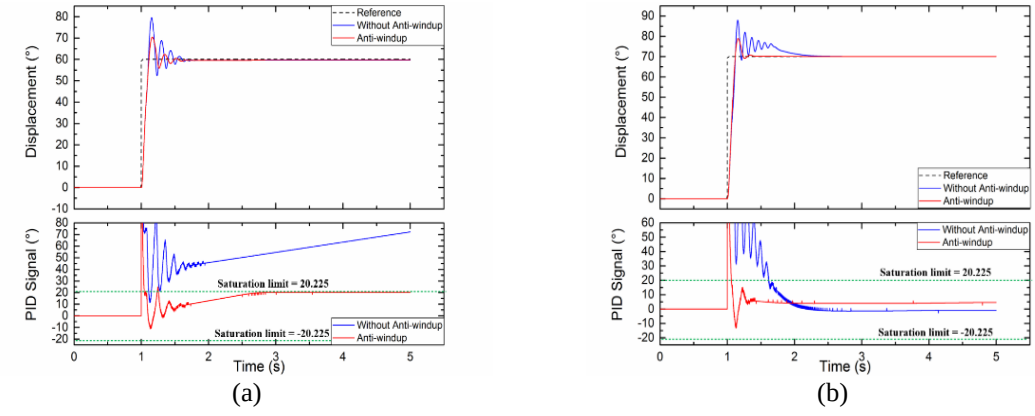

Figure 16. Effect of anti-windup at (a) reference 60° (fully aligned position) and (b) reference 70° (intermediate position)

4. CONCLUSION

In summary, the proposed modified PID controller with linearizer unit and anti-windup element outperformed the conventional PID controller in all analysis. The conventional PID controller does not perform well in the nonlinear rotary SRA system; however, by incorporating a linearizer unit and anti-windup into the

control scheme, significant improvements were achieved. The importance of both elements is emphasised in order to achieve better positioning results and serve as an important finding for future work. For the rotary SRA, excessive current excitation in the conventional PID controller resulted in significant overshoot and steady-state error. The modified PID controller, on the other hand, can provide the system with appropriate current values based on the linearizer unit to achieve lower error even when the rotor approaches fully aligned positions. When approaching these dead zones, torque decreases because the minimal torque refuses to move even when the aligned phase is excited. Furthermore, the modified PID controller with anti-windup prevented the PID signal from saturating. The anti-windup element helps to halt the integral action during the starting motion, reducing overshoot, and improving settling time. As a conclusion, at the fully aligned position 60°, the modified PID controller reduced positioning steady-state error by 4.3 times, maximum overshoot by 48.8%, and settling time by 25.3%. Both the modified PID and conventional PID controllers demonstrated zero steady-state error at the intermediate position of 70°, however the modified PID controller drastically improved the percentage overshoot by 54.5% and settling time by 75%.

ACKNOWLEDGEMENTS

The authors wish to express their gratitude to Motion Control Research Laboratory (MCon Lab), Center for Robotics and Industrial Automation (CeRIA), Centre for Research and Innovation Management (CRIM), Faculty of Electrical Engineering (FKE), and Universiti Teknikal Malaysia Melaka (UTeM) for supporting the research and publication. This research is supported by Ministry of Higher Education Malaysia **(**MOHE**)** under the Fundamental Research Grant Scheme (FRGS) grant no. FRGS/2018/FKE-CERIA/F00353.

REFERENCES

[1] E. Bostanci, M. Moallem, A. Parsapour, and B. Fahimi, "Opportunities and Challenges of Switched Reluctance Motor Drives for Electric Propulsion: A Comparative Study," *IEEE Transactions on Transportation Electrification*, vol. 3, no. 1, pp. 58–75, Mar. 2017, doi: 10.1109/TTE.2017.2649883.

[2] S. Vuddanti, V. Karknalli, and S. R. Salkuti, "Design and comparative analysis of three phase, four phase and six phase switched reluctance motor topologies for electrical vehicle propulsion," *Bulletin of Electrical Engineering and Informatics*, vol. 10, no. 3, pp. 1495-1504, Jun. 2021, doi: 10.11591/eei.v10i3.3054.

[3] P. Srinivas and K. Amulya, "Comparative Analysis of DITC Based Switched Reluctance Motor Using Asymmetric Converter and Four-Level Converter," *Bulletin of Electrical Engineering and Informatics*, vol. 5, no. 1, pp. 109-119, Mar. 2016, doi: 10.11591/eei.v5i1.555.

[4] S. Yang and Q. Xu, "A review on actuation and sensing techniques for MEMS-based microgrippers," *J Micro-Bio Robot*, vol. 13, no. 1, pp. 1–14, Oct. 2017, doi: 10.1007/s12213-017-0098-2.

[5] I. Yusri *et al.*, "Optimization of the force characteristic of rotary motion type of electromagnetic actuator based on finite element analysis," *Jurnal Teknologi*, vol. 78, no. 9, pp. 13-20, Aug. 2016, doi: 10.11113/jt.v78.7161.

[6] W. Ding, S. Yang, Y. Hu, S. Li, T. Wang, and Z. Yin, "Design Consideration and Evaluation of a 12/8 High-Torque Modular-Stator Hybrid Excitation Switched Reluctance Machine for EV Applications," *IEEE Transactions on Industrial Electronics*, vol. 64, no. 12, pp. 9221–9232, Dec. 2017, doi: 10.1109/TIE.2017.2711574.

[7] B. Li, X. Ling, Y. Huang, L. Gong, and C. Liu, "Predictive current control of a switched reluctance machine in the direct-drive manipulator of cloud robotics," *Cluster Comput*, vol. 20, no. 4, pp. 3037–3049, Dec. 2017, doi: 10.1007/s10586-017-0983-4.

[8] N. D. Veena and N. L. Raghuram, "Minimization of torque ripple using DITC with optimum bandwidth and switching frequency for SRM employed in electric vehicle," in *2017 International Conference on Smart grids, Power and Advanced Control Engineering (ICSPACE)*, Bangalore, India, Aug. 2017, pp. 143–148, doi: 10.1109/ICSPACE.2017.8343420.

[9] S. J. Evangeline, K. Venmathi, and S. Ajayan, "Speed control of switched reluctance motor using fractional order control," in *2017 International Conference on Innovations in Electrical, Electronics, Instrumentation and Media Technology (ICEEIMT)*, Coimbatore, India, Feb. 2017, pp. 367–372, doi: 10.1109/ICIEEIMT.2017.8116868.

[10] A. Mukherjee, P. Karmakar, S. Kumar Shome, S. Sen, and U. Datta, "Precision positioning system for long travel range and submicron resolution," in *2016 2nd International Conference on Control, Instrumentation, Energy & Communication (CIEC)*, Jan. 2016, pp. 83–87, doi: 10.1109/CIEC.2016.7513835.

[11] H. Nagy, M. Ruba, H. Hedesiu, and C. Martis, "Rapid control prototyping of a speed control strategy for a switched reluctance machine," in *2016 International Conference and Exposition on Electrical and Power Engineering (EPE)*, Romania, Oct. 2016, pp. 664–668, doi: 10.1109/ICEPE.2016.7781422.

[12] J. F. Pan, W. Wang, E. Cheung, N. Cheung, X. Wu, and B. Zhang, "Self-Tuning Position Control for the Linear Long-Stroke, Compound Switched Reluctance Conveyance Machine," *Int. J. Precis. Eng. Manuf.*, vol. 19, no. 3, pp. 387–394, Mar. 2018, doi: 10.1007/s12541-018-0046-7.

[13] L. Qiu, Y. Shi, J. Pan, and B. Zhang, "Robust Cooperative Positioning Control of Composite Nested Linear Switched Reluctance Machines With Network-Induced Time Delays," *IEEE Transactions on Industrial Electronics*, vol. 65, no. 9, pp. 7447–7457, Sep. 2018, doi: 10.1109/TIE.2017.2772186.

[14] Z. Su, C. Zhang, M. Wang, and Z. Dai, "Research on switched reluctance motor speed control system based on robust control," in *IECON 2017 - 43rd Annual Conference of the IEEE Industrial Electronics Society*, Beijing, China, Oct. 2017, pp. 6229–6232, doi: 10.1109/IECON.2017.8217082.

[15] S.-Y. Wang, F.-Y. Liu, and J.-H. Chou, "Design on Sliding Mode Controller with Adaptive Fuzzy Compensation for Switched Reluctance Motor Drive Systems," in *2016 International Symposium on Computer, Consumer and Control (IS3C)*, Xi'an, China, Jul. 2016, pp. 239–242, doi: 10.1109/IS3C.2016.71.

[16] W. Wang, N. Cheung, E. Cheng, B. Zhang, and J. F. Pan, "Position control for the linear compound switched reluctance machine," in *2016 International Symposium on Electrical Engineering (ISEE)*, Hong Kong, China, Dec. 2016, pp. 1–4, doi: 10.1109/EENG.2016.7846363.

[17] A. Xu, W. Zhang, and P. Ren, "Comparison of torque ripple reduction for switched reluctance motor based on DTC and DITC," in *2018 13th IEEE Conference on Industrial Electronics and Applications (ICIEA)*, Wuhan, China, May 2018, pp. 1727–1732, doi: 10.1109/ICIEA.2018.8397988.
[18] N. Yan, X. Cao, and Z. Deng, "Direct Torque Control for Switched Reluctance Motor to Obtain High Torque–Ampere Ratio," *IEEE Transactions on Industrial Electronics*, vol. 66, no. 7, pp. 5144–5152, Jul. 2019, doi: 10.1109/TIE.2018.2870355.
[19] Y. Zou, N. C. Cheung, and J. F. Pan, "An Adaptive High-Precision Tracking Controller for the Coupled Switched Reluctance Two-Finger Gripper," *IEEE Transactions on Magnetics*, vol. 51, no. 11, pp. 1–4, Nov. 2015, doi: 10.1109/TMAG.2015.2436399.
[20] J. F. Pan, Q. Li, L. Qiu, N. Cheung, X. Wu, and B. Zhang, "A fuzzy position controller for linear switched reluctance motor," *International Journal of Applied Electromagnetics and Mechanics*, vol. 55, no. 4, pp. 613–624, Jan. 2017, doi: 10.3233/JAE-170092.
[21] Y. Jiang, M. Wang, J. Duan, and J. Zhao, "High Precision Seeder Control System Based on Fuzzy Algorithm," in *2018 2nd IEEE Advanced Information Management,Communicates,Electronic and Automation Control Conference (IMCEC)*, Xi'an, China, May 2018, pp. 1754–1757, doi: 10.1109/IMCEC.2018.8469683.
[22] V. Pushparajesh, N. B. M, and H. B. Marulasiddappa, "Hybrid intelligent controller based torque ripple minimization in switched reluctance motor drive," *Bulletin of Electrical Engineering and Informatics*, vol. 10, no. 3, pp. 1193-1203, Jun. 2021, doi: 10.11591/eei.v10i3.3039.
[23] Y. Lee, D. Shin, W. Kim, and C. C. Chung, "Nonlinear H2 Control for a Nonlinear System With Bounded Varying Parameters: Application to PM Stepper Motors," *IEEE/ASME Transactions on Mechatronics*, vol. 22, no. 3, pp. 1349–1359, Jun. 2017, doi: 10.1109/TMECH.2017.2686901.
[24] M. N. Maslan, H. Kokumai, and K. Sato, "Development and precise positioning control of a thin and compact linear switched reluctance motor," *Precision Engineering*, vol. 48, pp. 265–278, Apr. 2017, doi: 10.1016/j.precisioneng.2016.12.009.
[25] M. N. Maslan, K. Sato, and T. Shinshi, "Position measurement and control of a thin and compact linear switched reluctance motor with a disposable-film mover," *Sensors and Actuators A: Physical*, vol. 285, pp. 80–88, Jan. 2019, doi: 10.1016/j.sna.2018.11.005.

BIOGRAPHIES OF AUTHORS

Mariam Md Ghazaly is an Associate Professor at the Department of Mechatronics, Faculty of Electrical Engineering, Universiti Teknikal Malaysia Melaka (UTeM), Malaysia. She received her B.Eng. Electrical Engineering and M.Eng. Electrical-Mechatronics and Automatic Control from Universiti Teknologi Malaysia, Malaysia in 2004 and 2005. In 2009 and 2012, she received M.Eng. and Ph.D. degree from the Tokyo Institute of Technology, Japan, in Mechano-Micro Engineering (Precision Engineering). She is a member of the Institute of Electrical and Electronics Engineers (IEEE), the Institution of Engineering and Technology (MIET), and a gradute member of Board of Engineers, Malaysia (BEM). Her research focuses on actuator design, precision engineering, and non-linear control algorithm. She can be contacted at email: mariam@utem.edu.my.

Siau Ping Tee is currently working as a system integrator in an oil and gas industry. He received his B.Eng. and M.Eng. in the field of in Mechatronics and Control System from Universiti Teknikal Malaysia Melaka (UTeM), Malaysia in 2017 and 2019. His research interest is in the field of control, robotics, and automation field. He has experiences in automation control for manufacturing and assembly processes. He can be contacted at email: deviant_79@hotmail.com.

Nasharuddin Zainal is an Associate Professor at the Faculty of Engineering and Built Environment, Universiti Kebangsaan Malaysia. He received the B.Eng. degree from Tokyo Institute of Technology in 1998, M.Eng. degree from the National University of Malaysia in 2003 and the Ph.D. degree from Tokyo Institute of Technology in 2010. He is also member of IEEE, corporate member of the Institution of Engineers Malaysia and certified professional Engineer of Board of Engineers Malaysia. His research is on image and video processing, pattern recognition, and robotics. He can be contacted at email: nasharuddin.zainal@ukm.edu.my.